THE ASTROPHYSICAL JOURNAL, 450:883–895, 1995 September 10

BOUND-BOUND TRANSITIONS IN STRONGLY MAGNETIZED HYDROGEN PLASMA

GEORGE G. PAVLOV[1]
Pennsylvania State University, Department of Astronomy and Astrophysics, 525 Davey Laboratory, University Park, PA 16802; pavlov@astro.psu.edu

AND

ALEXANDER Y. POTEKHIN[2]
Nordita, Blegdamsvej 17, DK-2100 Copenhagen Ø, Denmark; palex@astro.ioffe.rssi.ru
Received 1994 November 28; accepted 1995 March 22

ABSTRACT

Bound-bound absorption of polarized photons by hydrogen atoms is investigated for conditions expected in atmospheres of strongly magnetized neutron stars. Thermal motion of atoms across the strong magnetic field causes striking changes of the binding energies and oscillator strengths; these changes then lead to a new type of broadening of spectral lines. This magnetic broadening exceeds the collisional and Doppler broadenings by orders of magnitude, smearing the lines over wide, overlapping frequency bands. Low-energy components of the resulting spectra are due to strongly decentered atoms whose electrons are shifted from the protons by the electric field caused by the motion across the magnetic field. The absorption spectra depend significantly on the polarization and direction of radiation with respect to the magnetic field. The bound-bound transitions are expected to determine the spectra and the light curves of the soft X-ray/UV thermal-like radiation from middle-aged cooling neutron stars.

Subject headings: atomic processes — line: formation — line: profiles — magnetic fields — plasmas — stars: neutron

1. INTRODUCTION

With the development of observational capabilities of the space X-ray/UV observatories and ground-based telescopes, it is now feasible to detect radiation from surface layers of neutron stars with relatively low temperatures, $T \sim 10^5$–10^6 K (Ögelman 1995). Because of the huge magnetic fields of neutron stars, $B \sim 10^{11}$–10^{13} G, the ionization potentials of atoms are increased up to values $\sim Z^2$ Ry $\ln^2(\gamma/Z^2)$ at $\gamma \gg Z^2$ (e.g., Canuto & Ventura 1977), where $\gamma = \hbar\omega_B/(2\ \mathrm{Ry}) = B/2.35 \times 10^9$ G is the magnetic field in atomic units (a.u.), $\omega_B = eB/m_e c$ is the electron cyclotron frequency, Z is the effective ion charge, and $\mathrm{Ry} = m_e e^4/2\hbar^2 = 13.6$ eV is the Rydberg energy. This means that even light atoms, including hydrogen, are not completely ionized in neutron star atmospheres, and their contribution to the atmosphere opacity becomes the most important (Pavlov et al. 1995). Thus, in order to model neutron star atmospheres for further interpretation of the observational results, it is necessary to investigate the bound-bound and bound-free transitions of strongly magnetized atoms.

Such investigations have been undertaken (Forster et al. 1984; Ventura et al. 1992; Potekhin & Pavlov 1993, and references therein) for the simplest atom, hydrogen, assuming the center of mass of the atom to be fixed. However, it has recently been understood that the motion of atoms in strong magnetic fields changes their structure qualitatively (Vincke, Le Dourneuf, & Baye 1992). This occurs because the motion across the magnetic field induces an electric field which breaks the cylindrical symmetry and couples the internal structure of the atom to the center-of-mass motion. The energies and wave functions of the moving atom depend on the transverse component $K_\perp$ of a *generalized momentum* $\boldsymbol{K}$ that, contrary to the canonical and kinetic momenta, is conserved for a neutral atom moving in a magnetic field (Gorkov & Dzyaloshinskii 1967). When $K_\perp$ is small, the perturbation approach is applicable, and the coupling effect can be described in terms of an effective transverse mass of the atom (Vincke & Baye 1988; Pavlov & Mészáros 1993). This transverse mass always exceeds the mass of the atom without the magnetic field. It grows with the magnetic field, and it is generally higher for more excited atomic states. When $K_\perp$ increases beyond the applicability of the perturbation theory, the induced electric field causes decentering of the atom, i.e., the center of the electron cloud becomes substantially shifted from the proton. These decentered atoms have very unusual properties. For instance, their velocity decreases with increasing $K_\perp$ since the growth of $K_\perp$ goes not to acceleration of the atom but to larger decentering.

Qualitative effects of the coupling on the radiative transitions were discussed by Pavlov & Mészáros (1993). In particular, they showed that different dependence of different atomic levels on $K_\perp$ leads to an additional broadening of the spectral lines and photoionization edges. In strong magnetic fields, the corresponding *magnetic width* exceeds the Doppler and collisional widths by orders of magnitude, growing proportional to the gas temperature. Another important consequence of the coupling is that the oscillator strengths change with varying $K_\perp$ so that some transitions forbidden for the atom at rest become allowed for the moving atom. Thus, allowance for the coupling effects is necessary to calculate the atomic spectral opacity under realistic conditions.

Some aspects of the coupling effect on the bound-free transitions in strongly magnetized hydrogen have been analyzed by Bezchastnov & Potekhin (1994) and Ventura, Herold, & Kopi-

[1] On leave from A. F. Ioffe Physico-Technical Institute, St. Petersburg, Russia.

[2] Permanent address: A. F. Ioffe Physico-Technical Institute, St. Petersburg, Russia.

dakis (1995). The spectral dependence of the bound-bound transitions was discussed by Pavlov & Mészáros (1993) using the perturbation approach. Potekhin (1994) computed the oscillator strengths of the bound-bound transitions from the ground state of the hydrogen atom for a wide range of $K_\perp$.

In the present paper we investigate the bound-bound spectral profiles, and we take into account the dependences of both the energy and oscillator strength on the (arbitrarily large) transverse momentum $K_\perp$. In § 2 we recall the basic results on the structure of the moving atoms and derive general equations for the bound-bound absorption coefficients in a strongly magnetized plasma. The oscillator strengths for the hydrogen atom are presented in § 3 for three values of the magnetic field and for a wide range of $K_\perp$. Based on these results, we calculate in § 4 the spectral profiles of the bound-bound absorption for various values of the magnetic field, temperature, and density. The results obtained are summarized, and their astrophysical implications are discussed in § 5.

2. GENERAL EQUATIONS

2.1. *Quantum Mechanics of the Hydrogen Atom Moving in a Strong Magnetic Field*

A detailed discussion of the properties of the hydrogen atom moving in a strong magnetic field has been given by Vincke et al. (1992) and Potekhin (1994). We present here only some basic formulae essential for our further calculations of the absorption coefficients.

Let us consider a hydrogen atom moving with the generalized momentum $\boldsymbol{K}$ in a uniform magnetic field $\boldsymbol{B}$ directed along the z-axis. After separation of the center-of-mass motion, one arrives at the Schrödinger equation $H_{\rm rel}\psi = E\psi$ for the wave function ψ of the relative motion. The Hamiltonian can be presented in the form (Gorkov & Dzyaloshinskii 1967)

$$H_{\rm rel} = K_z^2/(2M) + p_z^2/(2\mu) + H_\perp - e^2/|\boldsymbol{r}_c + \boldsymbol{r}| , \qquad (1)$$

where $M = m_e + m_p$ and $\mu = m_e m_p/M$ are the total and reduced masses,

$$H_\perp = \frac{1}{2\mu}\left(\boldsymbol{p}_\perp + \frac{e}{2c}\boldsymbol{B}\times\boldsymbol{r}\right)^2 - \frac{e}{m_p c}\boldsymbol{B}(\boldsymbol{r}\times\boldsymbol{p}) \qquad (2)$$

is the transverse kinetic part of the Hamiltonian,

$$\boldsymbol{r}_c = \frac{c}{eB^2}\boldsymbol{B}\times\boldsymbol{K} \qquad (3)$$

is a typical shift of the magnetic (harmonic) potential well due to the electric field induced by the motion, and

$$\boldsymbol{r} = \boldsymbol{r}_e - \boldsymbol{r}_p - \boldsymbol{r}_c \qquad (4)$$

is the shifted relative coordinate ($\boldsymbol{r}_e$ and $\boldsymbol{r}_p$ are the electron and proton coordinates).

The eigenvalues of $H_\perp$ are the energies of the transverse motion of the proton and electron without the Coulomb field,

$$E_{Nm}^\perp = \frac{m_e}{\mu}\left(N + \frac{1}{2}\right)\hbar\omega_B - \frac{m_e}{m_p} m\hbar\omega_B , \qquad (5)$$

and the eigenfunctions are the Landau functions $\Phi_{Nm}(\boldsymbol{r}_\perp)$, where $N \geq 0$ is the Landau quantum number and $m \leq N$ is the z-projection of the angular momentum. Neither N nor m is conserved when the Coulomb interaction is taken into account in equation (1). However, it is convenient to expand the wave function $\psi(\boldsymbol{r})$ over the basis of the Landau functions $\Phi_{Nm}(\boldsymbol{r}_\perp)$:

$$\psi_\kappa(\boldsymbol{r}, \boldsymbol{K}_\perp) = \sum_{N'm'} \Phi_{N'm'}(\boldsymbol{r}_\perp) g_{N'm',\kappa}(z) . \qquad (6)$$

The states of the atom moving in a strong magnetic field ($\gamma \gg 1$) may be numbered as $\kappa = (Nm\nu)$ (Potekhin 1994) by analogy with the case of no motion (Forster et al. 1984). The numbers N and m are those of the leading term of the expansion (6), while $\nu = 0, 1, \ldots$ numerates the longitudinal energy levels

$$E_{Nm\nu}^\parallel(K_\perp) = E_{Nm\nu}(K_\perp) - E_{Nm}^\perp . \qquad (7)$$

The z-parity of the wave function is $(-1)^\nu$. The binding energy is $\chi_\kappa(K_\perp) = E_{00}^\perp - E_\kappa(K_\perp)$, and the total energy of the atom measured from the common continuum is $\epsilon_\kappa(\boldsymbol{K}) = K_z^2/(2M) - \chi_\kappa(K_\perp)$. In strong magnetic fields ($\gamma \gtrsim 1$), the truly bound states ($\chi_\kappa > 0$) are those with $N = 0$ and $-m$ not large, whereas other states are mixed with the continuum and are subject to autoionization.

The behavior of the longitudinal energies $E_\kappa^\parallel(K_\perp)$ is different for $K_\perp \ll K_c$ and $K_\perp \gg K_c$, where $K_c \approx [2M|E_\kappa^\parallel(0)|]^{1/2}$. At small transverse momenta, these energies grow logarithmically with the field strength for the tightly bound states ($\nu = 0$) and approach the levels of the field-free atom for the hydrogen-like states ($\nu \geq 1$), while their dependence on $K_\perp$ is

$$E_\kappa(K_\perp) = E_\kappa(0) + K_\perp^2/(2M_\kappa^\perp) . \qquad (8)$$

The "transverse mass" $M_\kappa^\perp$ exceeds the total mass M and grows with the field strength (Vincke & Baye 1988; Pavlov & Mészáros 1993). At large $K_\perp$, the atom becomes decentered; that is, the electron becomes shifted from the proton by $\sim r_c = (a_0^2/\hbar)K_\perp/\gamma$, where a_0 is the Bohr radius. The longitudinal energies of the decentered states tend to zero with increasing $K_\perp$ as $E_\kappa^\parallel \sim -e^2/r_c$ (Burkova et al. 1976). Some representative examples of the dependence $\chi_{0m\nu}(K_\perp)$ are shown in the bottom panels of Figures 1 and 2.

Applying the Schrödinger variational principle to the expansion (6), one obtains a set of coupled second-order linear differential equations for the functions $g_{N'm',\kappa}(z)$, which are to be solved numerically (see Potekhin 1994 for details). After these functions are found for some initial $|\kappa, \boldsymbol{K}_\perp\rangle$ and final $|\kappa', \boldsymbol{K}'_\perp\rangle$ atomic states, one can calculate the oscillator strengths of the radiative transitions between them, $f_{\kappa\kappa'}^\beta(\boldsymbol{K}_\perp, \boldsymbol{q})$, where β is the polarization index of incident radiation and $\boldsymbol{q} = \boldsymbol{K}'_\perp - \boldsymbol{K}_\perp$ is the photon momentum.

The bound-bound transitions between the states with $N' = 0$ can be treated in the dipole approximation ($\boldsymbol{q} \to 0$) because the atomic sizes l_κ are much smaller than the corresponding photon wavelengths λ ($\gtrsim 2\pi\hbar c/\chi_\kappa$). This follows from estimates of the binding energies and sizes of the hydrogen atom in a strong magnetic field (Potekhin 1994). In the centered states, the atom is stretched along the field, so that the maximum size $l_\kappa \approx l_z$. For the tightly bound centered states, $l_z \sim 0.5\hbar(m_e|E_\kappa^\parallel|)^{-1/2}$, $|E_\kappa^\parallel| \leq \chi_\kappa$, and $l_\kappa/\lambda \lesssim (\chi_\kappa/{\rm Ry})^{1/2}(\alpha/2^{5/2}\pi)$, where $\alpha = 1/137$ is the fine-structure constant. Since $\chi_\kappa \lesssim 20$ Ry for the states and field strengths under consideration, we see that $l_\kappa/\lambda \ll 1$. For the hydrogen-like centered states, $l_z \sim 0.8e^2/|E^\parallel|$, and $l_\kappa/\lambda \lesssim 0.8\alpha/2\pi \ll 1$. In the decentered states, the atom is stretched mostly in the direction toward the relative guiding center, $l_\kappa \sim l_x \approx r_c$, while $|E^\parallel| \sim e^2/r_c$. Hence, $l_\kappa/\lambda \lesssim \alpha/2\pi \ll 1$, and the dipole approximation proves to be valid for these states as well. The above consideration is supported by our numerical study of the bound-free

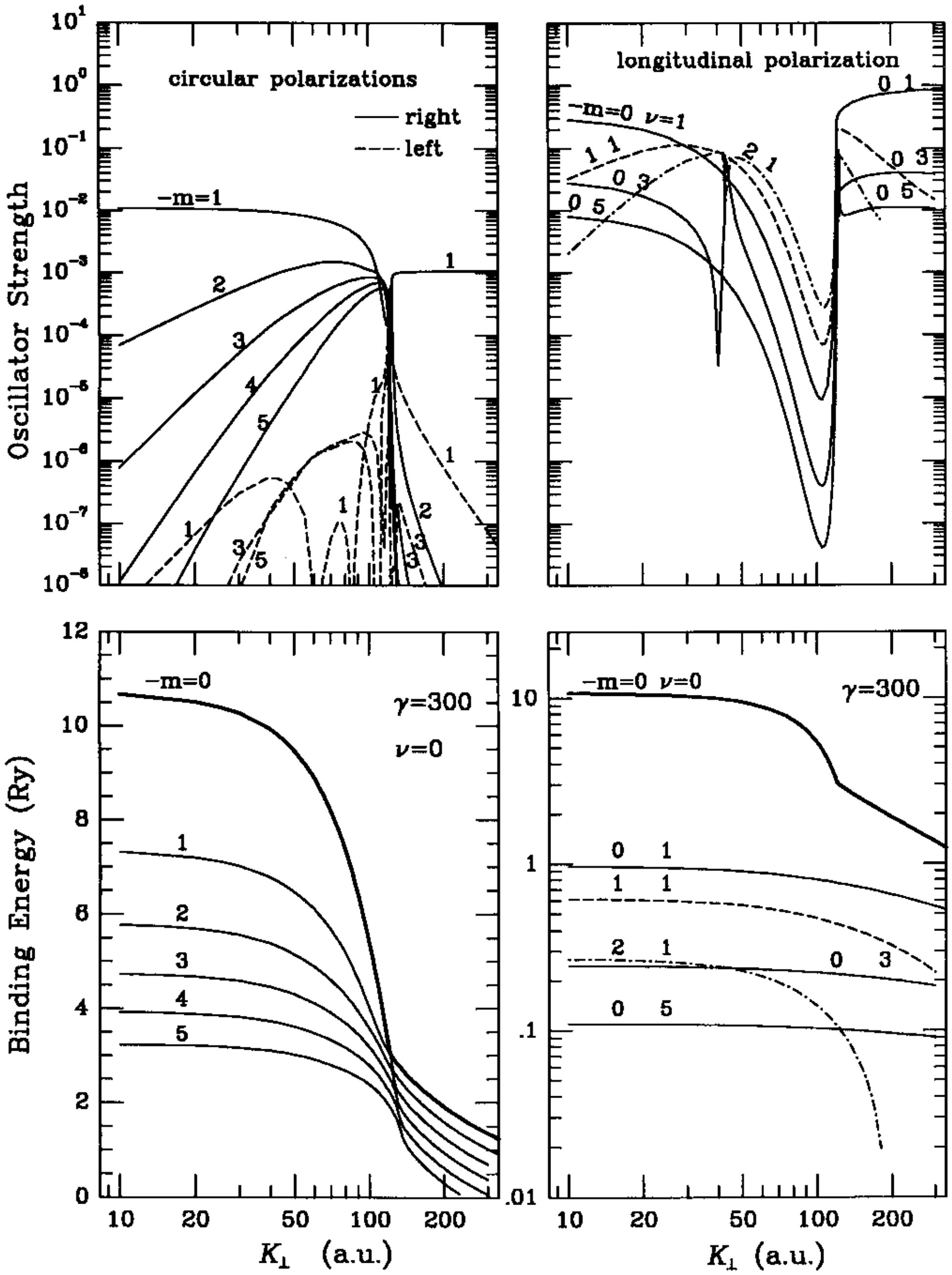

FIG. 1.—Binding energies χ_κ and oscillator strengths $f^{\beta}_{\kappa\kappa'}$ at $B = 7 \times 10^{11}$ G vs. transverse component of generalized momentum $\boldsymbol{K}$. The upper left-hand panel demonstrates the oscillator strengths of transitions from the ground state $\kappa = |0\,0\,0\rangle$ to the tightly bound states $\kappa' = |0\,m\,0\rangle$ for photons circularly polarized in the plane perpendicular to the magnetic field ($\beta = \pm 1$); the binding energies of the states are shown in the lower left-hand panel. The right-hand panels show the binding energies of the odd hydrogen-like states $|0\,m\,\nu\rangle$ ($\nu = 1, 3, 5$) and the oscillator strengths of the transitions $|000\rangle \rightarrow |0m\nu\rangle$ for photons linearly polarized along the magnetic field ($\beta = 0$).

transitions in strong magnetic fields (Potekhin & Pavlov 1993). While at high frequencies ($\omega \gtrsim \omega_B$) the effects of nondipole interactions may change transition rates by orders of magnitude, these effects become negligible near the threshold frequency ($\omega \sim \chi/\hbar$).

In the dipole approximation, the most convenient set of the basic polarizations consists of the longitudinal polarization, $\beta = 0$, with the polarization vector $\boldsymbol{e}_0 = \boldsymbol{e}_z$ along the magnetic field and right ($\beta = +1$) and left ($\beta = -1$) circular polarizations with polarization vectors $\boldsymbol{e}_{\pm 1} = (\boldsymbol{e}_x \pm i\boldsymbol{e}_y)/2^{1/2}$ in the plane perpendicular to the magnetic field. The oscillator strengths for these polarizations are

$$f^{\beta}_{\kappa\kappa'}(K_\perp) = \frac{\hbar\omega}{\mathrm{Ry}} \left| \frac{D^{-\beta}_{\kappa'\kappa}(K_\perp)}{a_0} \right|^2 , \tag{9}$$

where ω is the circular frequency and $D_{\kappa'\kappa}$ is the cyclic component of the dipole matrix element

$$D_{\kappa'\kappa}(K_\perp) = \langle \kappa', \boldsymbol{K}_\perp | \boldsymbol{r} | \kappa, \boldsymbol{K}_\perp \rangle . \tag{10}$$

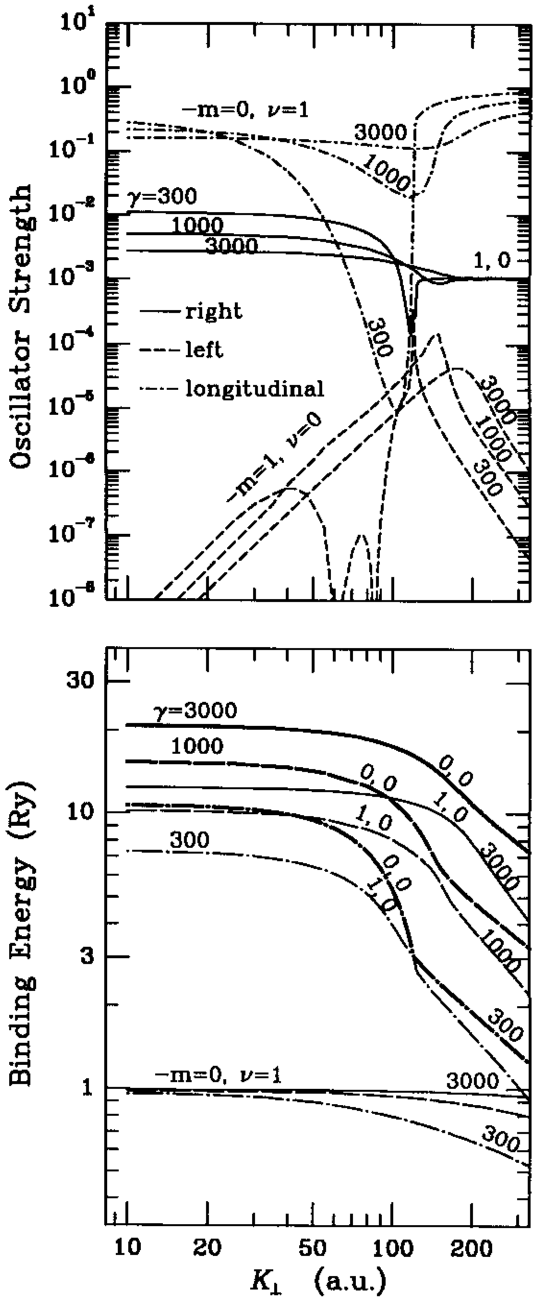

FIG. 2.—Oscillator strengths of main transitions from the ground state, $|000\rangle \to |001\rangle$ for the longitudinal polarization and $|000\rangle \to |0-10\rangle$ for the circular polarizations, for three values of the magnetic field: $\gamma = B/(2.35 \times 10^9\ \mathrm{G}) = 300$, 1000, and 3000 (*upper panel*). Behavior of the energy levels involved is shown in the lower panel.

Using the expansion (6) and the well-known relations for $r_{\pm 1}\Phi_{Nm}(r_\perp)$ (e.g., Potekhin & Pavlov 1993), $D^\beta_{\kappa'\kappa}$ can be easily reduced to a sum of one-dimensional (longitudinal) quadratures.

The "coordinate form" (10) of the interaction matrix element has some advantages for numerical treatment as compared to the alternative "velocity form" (see Potekhin & Pavlov 1993 and Potekhin 1994). Nevertheless, we employed both forms in our calculations, using coincidence of the results as a test of numerical accuracy.

2.2. *Absorption Coefficient*

The absorption coefficient for radiation with polarization β and wavevector $\boldsymbol{q}/\hbar$ reads, in the dipole approximation,

$$\kappa^\beta_{\kappa\kappa'}(\omega) = \frac{2\pi^2 e^2}{m_e c}\,(1 - e^{-\hbar\omega/k_B T}) \int d^3K\, N_\kappa(\boldsymbol{K}) \times f^\beta_{\kappa\kappa'}(K_\perp)\phi_{\kappa\kappa'}(K_\perp;\, \omega - \omega_{\kappa'\kappa})\,, \quad (11)$$

where k_B is the Boltzmann constant, $N_\kappa(\boldsymbol{K})$ is the distribution of the number density of atoms in the initial state $|\kappa, \boldsymbol{K}\rangle$, $\hbar\omega_{\kappa'\kappa} = \epsilon_{\kappa'}(\boldsymbol{K}') - \epsilon_\kappa(\boldsymbol{K})$, $\boldsymbol{K}' = \boldsymbol{K} + \boldsymbol{q}$, and $\phi_{\kappa\kappa'}(K_\perp;\ \Delta\omega)$ describes a normalized profile of the spectral line

$$\int_{-\infty}^{+\infty} \phi_{\kappa\kappa'}(K_\perp;\, \Delta\omega)\, d(\Delta\omega) = 1\,. \quad (12)$$

Since the energy $\chi_\kappa(K_\perp)$ tends to a constant value at $K_\perp \to \infty$, the normalization integral for the Boltzmann distribution $N_\kappa(\boldsymbol{K}) \propto \exp[-\epsilon_\kappa(\boldsymbol{K})/k_B T]$ diverges. The divergence is eliminated if nonideality of the gas is taken into account. At high $K_\perp$, the binding energies become small, and atomic sizes become large. This means that the atom can be easily destroyed by surrounding particles, so that very high $K_\perp$ should not contribute to the corresponding integrals. One meets the same situation in the problem of calculating the partition function in real gases; the sum over atomic levels diverges unless one takes into account that highly excited states are destroyed. A convenient approach to allow for this effect is the so-called occupation probability formalism described in detail by Hummer & Mihalas (1988). In this approach, the Boltzmann exponent is multiplied by the occupation probability w_κ which accounts for reduction of the number density N_κ of atoms in the κth state due to interparticle interactions. Generalizing the approach to the case of the $K_\perp$-dependent atomic structure, one can write

$$N_\kappa(\boldsymbol{K}) \propto w_\kappa(K_\perp) \exp[-\epsilon_\kappa(\boldsymbol{K})/k_B T]\,. \quad (13)$$

In this paper we consider a well-ionized hydrogen gas, in which atoms are destroyed mainly by electric microfields of bare protons. We assume that the atomic state $|\kappa, \boldsymbol{K}\rangle$ is destroyed if an alien proton approaches the atom to a distance comparable with a typical distance $l_\kappa(K_\perp)$ between the electron and the nucleus. This occurs when the proton gets into some "interaction volume" proportional to $[l_\kappa(K_\perp)]^3$. In the nonmagnetic case, the "nearest neighbor" occupation probabilities are recovered (see Hummer & Mihalas 1988) by setting the proportionality coefficient equal to $256\pi/3$. By analogy, we adopt in the magnetic case

$$w_\kappa(K_\perp) = \exp\{-(4\pi/3)[4 l_\kappa(K_\perp)]^3 N_p\}\,, \quad (14)$$

where N_p is the proton number density, $l_\kappa(K_\perp) = (l_x^2 + l_y^2 + l_z^2)^{1/2}$, and l_x, l_y, l_z are atomic sizes along the corresponding axes calculated and discussed previously (Potekhin 1994). Since $l_x \sim r_c$ for the decentered states, $w_\kappa(K_\perp)$ decreases rapidly at $K_\perp > \gamma\hbar/a_0$.

Equation (13) can now be rewritten as

$$N_\kappa(\boldsymbol{K}) = N_\kappa \mathcal{F}_\parallel(K_z)\mathcal{F}_\perp(K_\perp)\,, \quad (15)$$

where N_κ is the number density of atoms on the level κ,

$$\mathcal{F}_\parallel(K_z) = (2\pi M k_B T)^{-1/2} \exp[-K_z^2/(2M k_B T)] \quad (16)$$

and

$$\mathscr{F}_\perp(K_\perp) = A_\kappa^{-1} w_\kappa(K_\perp) \exp[\chi_\kappa(K_\perp)/k_B T] \tag{17}$$

are the distributions over longitudinal and transverse momenta, and

$$A_\kappa = 2\pi \int_0^\infty dK_\perp K_\perp w_\kappa(K_\perp) \exp[\chi_\kappa(K_\perp)/k_B T] \tag{18}$$

is the normalization constant.

Since only those atoms contribute to the bound-bound absorption whose final state is not destroyed by the proton microfields, one should multiply $N_\kappa(\boldsymbol{K})$ in equation (11) by a correction factor $w_{\kappa'}(K_\perp)/w_\kappa(K_\perp)$ (cf. Stehlé & Jacquemot 1993). Then, from equations (11) and (15)–(17), one obtains the absorption coefficient for the transition $\kappa \to \kappa'$:

$$\begin{aligned} \kappa^\beta_{\kappa\kappa'}(\omega) = \frac{2\pi^2 e^2}{m_e c}\left[1 - \exp\left(-\frac{\hbar\omega}{k_B T}\right)\right] \frac{N_\kappa}{A_\kappa} \int d^2 K_\perp \\ \times \phi_{\kappa\kappa'} \int_{-\infty}^{\infty} dK_z \mathscr{F}_\parallel(K_z) w_{\kappa'}(K_\perp) \exp\left[\frac{\chi_\kappa(K_\perp)}{k_B T}\right] f^\beta_{\kappa\kappa'}(K_\perp) \\ \times \phi_{\kappa\kappa'}\left[K_\perp; \omega - \frac{\chi_\kappa(K_\perp) - \chi_{\kappa'}(K_\perp) + \boldsymbol{q}\cdot \boldsymbol{V}_{\kappa'}(\boldsymbol{K})}{\hbar}\right]. \end{aligned} \tag{19}$$

Here we took into account that $\epsilon_{\kappa'}(\boldsymbol{K} + \boldsymbol{q}) \approx \epsilon_{\kappa'}(\boldsymbol{K}) + \boldsymbol{q} \cdot \boldsymbol{V}_{\kappa'}(\boldsymbol{K})$, where

$$\boldsymbol{V}_{\kappa'}(\boldsymbol{K}) = \frac{d\epsilon_{\kappa'}(\boldsymbol{K})}{d\boldsymbol{K}} = \frac{K_z}{M}\frac{\boldsymbol{B}}{B} - \frac{d\chi_{\kappa'}(K_\perp)}{dK_\perp}\frac{\boldsymbol{K}_\perp}{K_\perp} = V^\parallel \frac{\boldsymbol{B}}{B} + V^\perp_{\kappa'}(K_\perp)\frac{\boldsymbol{K}_\perp}{K_\perp} \tag{20}$$

is the velocity of the atom at given $\boldsymbol{K}$.

2.3. *Magnetic and Collisional Broadening*

One can see from Figures 1 and 2 that (at least, at $K_\perp < K_c$) the distance between the atomic levels decreases with increasing transverse momentum $K_\perp$. At temperatures and magnetic fields typical for the neutron star atmospheres, this variation of the transition energies is comparable to the binding energies, and thermal motion of the atoms across the magnetic field results in a great redward broadening of the spectral lines (Pavlov & Mészáros 1993). It should be stressed that this *magnetic broadening* is solely due to the coupling of the internal atomic structure to the center-of-mass motion (to different dependences of χ_κ and $\chi_{\kappa'}$ on $K_\perp$); it is quite different from the Doppler broadening which results from the Doppler shift $\boldsymbol{q} \cdot \boldsymbol{V}_{\kappa'}(\boldsymbol{K})$ in the argument of the spectral line profile $\phi_{\kappa\kappa'}$ in equation (19).

In wide frequency ranges in which the magnetic broadening is more important than the collisional and Doppler broadenings, one can substitute $\hbar\delta[\hbar\omega - \chi_\kappa(K_\perp) + \chi_{\kappa'}(K_\perp)]$ for the profile $\phi_{\kappa\kappa'}$. Then equation (19) yields

$$k^\beta_{\kappa\kappa'}(\omega) = \sum_i k^{\beta,i}_{\kappa\kappa'}(\omega), \tag{21}$$

where the index i numerates roots K^i_ω of the equation

$$\chi_\kappa(K_\omega) - \chi_{\kappa'}(K_\omega) = \hbar\omega, \tag{22}$$

and

$$k^{\beta,i}_{\kappa\kappa'}(\omega) = \frac{4\pi^3 e^2 N_\kappa}{m_e c A_\kappa}(1 - e^{-\hbar\omega/k_B T}) K^i_\omega \left|\frac{dK^i_\omega}{d\omega}\right| \times w_{\kappa'}(K^i_\omega) \exp\left[\frac{\chi_\kappa(K^i_\omega)}{k_B T}\right] f^\beta_{\kappa\kappa'}(K^i_\omega). \tag{23}$$

Notice that the derivative in this equation can be expressed in terms of the transverse velocities of the atom: $dK^i_\omega/d\omega = \hbar/[V^\perp_{\kappa'}(K^i_\omega) - V^\perp_\kappa(K^i_\omega)]$.

One can see from Figures 1 and 2 that the number of roots of equation (22) is different for different pairs $\kappa\kappa'$, and it depends on the frequency ω for a given pair. For instance, for the transitions from the ground level $\kappa = |0\,0\,0\rangle$ to the hydrogen-like levels $\kappa' = |0\,0\,\nu\rangle$, the transition frequency decreases monotonically with increasing $K_\perp$, tending to zero at $K_\perp \to \infty$. This means that equation (22) has no roots at $\omega > \omega_0$ [$k^\beta_{\kappa\kappa'}(\omega) = 0$], and it has only one root for each $\omega < \omega_0$, where $\hbar\omega_0 = \chi_\kappa(0) - \chi_{\kappa'}(0)$. If we consider the transitions from the ground level to the excited tightly bound levels $\kappa' = |0\,m\,0\rangle$, the transition frequency first decreases with $K_\perp$ until it reaches a minimum value ω_c at $K_\perp = K_c$ and then grows monotonically to a value ω_∞ ($< \omega_0$) at $K_\perp \to \infty$. In this case, equation (22) has one root for $\omega_\infty < \omega < \omega_0$, two roots for $\omega_c < \omega < \omega_\infty$, and it has no roots at $\omega < \omega_c$ and $\omega > \omega_0$.

If only the magnetic broadening is taken into account, spectral profiles have infinitely sharp edges at $\omega = \omega_0$, ω_c, and ω_∞. Moreover, the slopes of the curves $\chi_\kappa(K_\perp)$ and $\chi_{\kappa'}(K_\perp)$ are equal at $K_\perp = K_c$ and at $K_\perp \to \infty$, which means that the absorption coefficient diverges at $\omega = \omega_c$ and $\omega = \omega_\infty$. Thus, to describe behavior of the absorption coefficient around ω_0, ω_c, and ω_∞, one has to take into account the Doppler and/or collisional broadening.

The Doppler broadening in the strong magnetic field depends on the angle θ between the wavevector and the magnetic field, $\Gamma_D = (\Gamma_D^\parallel \cos^2\theta + \Gamma_D^\perp \sin^2\theta)^{1/2}$ (Pavlov & Mészáros 1993). The longitudinal Doppler width coincides with that without magnetic field, $\Gamma_D^\parallel = \omega_{\kappa'\kappa}(2kT/Mc^2)^{1/2} \simeq 9.6 \times 10^{-5} T_5^{1/2} \omega_{\kappa'\kappa}$, where $T_5 = T/(10^5\ \mathrm{K})$. The transverse Doppler width is usually much smaller than the longitudinal one because of the increased "transverse mass" of the atom.

Collisional broadening in the strongly ionized plasma is caused mainly by interactions of the atom with electric fields of charged particles. Interaction with slowly moving ions can be considered as quasi-static; to take it into account, one should find the absorption coefficient for the atom placed in a given (static) electric field and then average it with a proper distribution of the electric microfields. Interaction with faster electrons can be described in the impact approximation which implies that the duration of collisions is small compared with the mean time between collisions so that one can consider the collisions to be instantaneous. Generally, impact broadening becomes more important than quasi-static broadening at higher temperatures and lower densities.

The relative importance of the Doppler, quasi-static, and impact broadenings depends on the values of temperature, density, and magnetic field and on the specific transition. In different layers of the neutron star atmospheres any one of the three broadening mechanisms may be more important than the other two. However, since a detailed analysis of the spectral shape around the frequencies ω_0, ω_∞, and ω_c is not the goal of this paper and since the broadening additional to the magnetic broadening is introduced only to avoid the infinitely sharp edges and singularities, we will take into account only impact broadening. An analysis shows that impact broadening seems to dominate the Doppler and quasi-static broadenings for a wide range of realistic parameters; besides, it can more easily be incorporated into calculations of the spectral line profiles than two other broadening mechanisms.

Impact broadening can be described by the Lorentzian spectral profile

$$\phi_{\kappa\kappa'}(K_\perp;\Delta\omega)=\frac{\Gamma_{\kappa\kappa'}(K_\perp)}{2\pi}\left[(\Delta\omega)^2+\frac{\Gamma^2_{\kappa\kappa'}(K_\perp)}{4}\right]^{-1}. \quad (24)$$

The absorption coefficient with allowance for both magnetic and impact broadening can be written as the convolution

$$k^{\beta}_{\kappa\kappa'}(\omega)=\int d\omega'\sum_i \phi_{\kappa\kappa'}(K^i_{\omega'},\omega-\omega')\,k^{\beta,i}_{\kappa\kappa'}(\omega'), \quad (25)$$

where the integration is performed over those ω' for which a solution $K^i_{\omega'}$ of equation (22) exists. Thus, we will use equations (25), (24), and (23) to calculate the spectral profiles of the absorption coefficient. Calculation of the width $\Gamma_{\kappa\kappa'}(K_\perp)$ is described in the Appendix.

3. TRANSITION ENERGIES AND OSCILLATOR STRENGTHS

Let us consider radiative transitions from the ground state $\kappa=|0\;0\;0\rangle$ of the hydrogen atom to excited states $\kappa'=|0\;m'\;\nu'\rangle$. Transitions to states with $N'>0$ are of no practical importance in the strongly magnetized neutron star atmospheres (at $\hbar\omega_B \gg k_B T$) because there are almost no quanta at the corresponding frequencies. The binding energies, transition frequencies, and oscillator strengths strongly vary with the transverse momentum $K_\perp$, as illustrated in Figures 1 and 2. When $K_\perp=0$, the dipole selection rules allow only transitions to the states $|0\;0\;\nu'\rangle$, with $\nu'=1, 3, 5, \ldots$, for the longitudinal polarization ($\beta=0$), and to the state $|0\;-1\;0\rangle$ for the right circular polarization ($\beta=+1$). Transitions for the left circular polarization ($\beta=-1$) are allowed only to the excited Landau level (to the state $|1\;1\;0\rangle$). The selection rules change drastically when $K_\perp\neq 0$ owing to the breakdown of the axial symmetry. First, transitions to $|0\;m'\;\nu'\rangle$ with $m'=-1,-2,-3,\ldots$ (and odd ν') are no longer forbidden for $\beta=0$; for example, the oscillator strengths for the transitions to $|0\;-1\;1\rangle$ and $|0\;-2\;1\rangle$ are shown in the upper right-hand panel of Figure 1. Second, transitions for $\beta=-1$ become allowed to the states with $N=0$ (examples are shown by the dashed curves in the upper left-hand panel of Fig. 1 and the upper panel of Fig. 2). Third, for both $\beta=+1$ and $\beta=-1$, transitions to the states $|0\;m'\;0\rangle$ become allowed for any negative m'. The oscillator strengths for the transitions to various tightly bound states are shown in the upper panels of Figures 1 (*left*) and 2 by solid lines. For $\beta=\pm1$ the transitions are formally allowed also to the hydrogen-like states with $\nu'=2, 4, \ldots$, but the oscillator strengths are negligibly small everywhere except for a narrow resonance region at large $K_\perp$. The complicated, nonmonotonic behavior of the oscillator strengths in Figures 1 and 2 is associated with anticrossings of the energy levels, as one can see from a comparison of the upper panels of Figures 1 and 2 with the lower ones (see Potekhin 1994 for more numerical examples and discussion).

The curve corresponding to the final state $|0\;-2\;1\rangle$ (Fig. 1, lower right-hand panel) is truncated at the point at which $\chi_{0-21}=0$. The reason is that the states with $\chi_{\kappa'}<0$ are subject to autoionization. We do not consider this process in the present work and do not include autoionizing states in calculations of the absorption coefficients.

Figure 1 also demonstrates the $K_\perp$-dependence of the binding energies and the oscillator strengths for different transitions at $\gamma=300$. In the mixing range, $K_\perp\sim K_c\sim 100$–150 a.u., where the energies of the tightly bound levels suffer (anti)crossings, behavior of the oscillator strengths is rather complicated. For the circular polarizations $\beta=\pm1$, transitions to several states $|0\;m'\;0\rangle$ are almost equally important at $K_\perp\sim K_c$, whereas at $K_\perp\ll K_c$ and $K_\perp\gg K_c$, only one of these transitions survives. The transition frequency $\omega(K_\perp)$ for a given transition $|0\;0\;0\rangle\rightarrow|0\;m'\;0\rangle$ decreases with increasing $K_\perp$ from ω_0 at $K_\perp=0$ down to a minimum frequency $\omega_c=\omega(K_c)$ and then grows again up to $\omega_\infty=|m'|\,\omega_{B_p}$, where $\omega_{B_p}=(m_e/m_p)\omega_B$ is the proton cyclotron frequency. Since $\omega(K_\perp)-\omega_c\propto(K_\perp-K_c)^2$ near the turning point, the absorption coefficient calculated without accounting for the collisional and/or Doppler broadening acquires a square-root singularity (cf. eq. [23]),

$$k^{\beta,i}_{\kappa\kappa'}(\omega)\propto|dK^i_\omega/d\omega|\propto(\omega-\omega_c)^{-1/2}. \quad (26)$$

This singularity is integrable, and it is eliminated by the collisional broadening.

At $K_\perp\rightarrow\infty$ all binding energies tend to constant values (see eq. [A21]), and $\omega(K_\perp)-\omega_\infty\simeq(|m'|/2)(e\hbar\gamma/a_0^2)^2K_\perp^{-3}$. As a result, a singular factor appears in equation (23) for the corresponding i,

$$K^i_\omega\left.\frac{dK^i_\omega}{d\omega}\right|\propto(\omega_\infty-\omega)^{-5/3}. \quad (27)$$

This (nonintegrable) singularity is suppressed by the occupation probability exponentially decreasing at $K_\perp\rightarrow\infty$: $w_{\kappa'}(K^i_\omega)\sim\exp\{-(256\pi/3)(N_p a_0^3)(|m|/\gamma)[\mathrm{Ry}/\hbar(\omega_\infty-\omega)]\}$.

For the longitudinal polarization, the transition frequency decreases monotonically down to zero with increasing $K_\perp$ (see Fig. 1, lower right-hand panel): $\omega(K_\perp)\simeq(e^2/\hbar a_0)(\gamma\hbar/a_0)^{3/2}\nu' K_\perp^{-3/2}$.

This means that a divergent factor appears in equation (23) at $\omega\rightarrow0$:

$$K^i_\omega\left|\frac{dK^i_\omega}{d\omega}\right|\propto\omega^{-7/3}. \quad (28)$$

This divergence is also suppressed by the occupation probability of the excited level: $w_{\kappa'}(K^i_\omega)\sim\exp\,[-(256\pi/3)(N_p a_0^3)\nu'^2(2\,\mathrm{Ry}/\hbar\omega)]$. Examples of the $K_\perp$-dependences of the occupation probabilities for the tightly bound states $|0\;0\;0\rangle$ and $|0\;1\;0\rangle$ and the hydrogen-like state $|0\;0\;1\rangle$ are shown in Figure 3. In the considered density range, the occupation probabilities decrease rapidly at $K_\perp>\gamma\hbar/a_0$ for the tightly bound states and at considerably lower $K_\perp$ for the lowest odd state $|0\;0\;1\rangle$ (other odd states practically do not exist already at $\rho=0.01$ g cm^{-3}).

4. SPECTRAL SHAPES

We used the transition energies and oscillator strengths discussed in § 3 to compute the absorption coefficients according to equations (21)–(25). The occupation probability is given by equation (14), and the collisional width is given by equation (A17). Some typical examples of the width are shown in Figure 4.

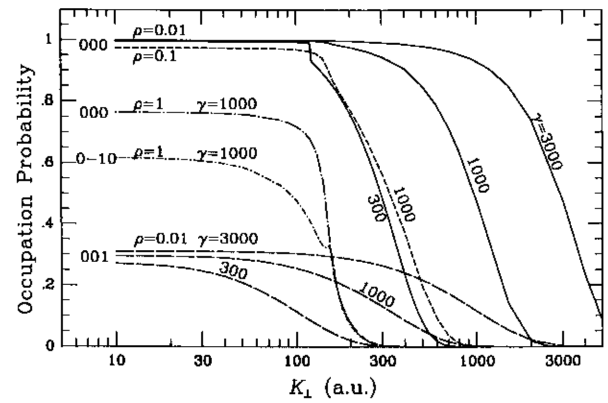

FIG. 3.—Occupation probabilities $w_\kappa(K_\perp)$ for the states $\kappa = |0\,0\,0\rangle, |0\,0\,1\rangle$, and $|0\ -1\ 0\rangle$, for $\gamma = 300$, 1000, and 3000, and for the densities $\rho = 0.01$, 0.1, and 1 g cm^{-3}.

When we take into account that, as a rule, the neutral fraction $\xi = 1 - N_p/N$ is small in neutron star atmospheres, we replace the proton number density N_p in equation (14) by the total number density N. Then the partial fractions N_κ/N become independent of ξ, and the absorption coefficient becomes directly proportional to ξ. Therefore, we can calculate the absorption per unit neutral fraction, $k^{\beta}_{\kappa\kappa'}(\omega)/\xi$. Figure 5 presents this quantity for the main transitions from the ground state, $|0\ 0\ 0\rangle \rightarrow |0\ 0\ 1\rangle$ for $\beta = 0$ and $|0\ 0\ 0\rangle \rightarrow |0\ -1\ 0\rangle$ for $\beta = \pm 1$, at $B = 2.35 \times 10^{12}$ G. The asymmetric peaks around $\hbar\omega_0 = 14.3$ Ry for $\beta = 0$ and $\hbar\omega_0 = 5.1$ Ry for $\beta = +1$ are produced by atoms with small transverse momenta, $K_\perp \ll K_c \sim 150(\hbar/a_0)$. The absorption profiles decrease exponentially redward of ω_0; this magnetic broadening is due to different dependences of the ground and excited levels on $K_\perp$ (see Figs. 1 and 2). The decrease of the corresponding oscillator strengths with increasing $K_\perp$ reduces the magnetic widths making the profiles sharper than predicted by the simpler transverse-mass (perturbation) approximation (see Pavlov & Mészáros 1993); this effect is more pronounced at higher temperatures so that the profiles at $T = 10^6$ K ($k_B T = 6.3$ Ry) are only slightly wider than those at $T = 10^{5.5}$ K ($k_B T = 2.0$ Ry)—compare the solid curves 1 and 2. Additional narrowing for $\beta = 0$ at higher densities (compare the solid curves 1 and 3) is caused by the decrease of the occupational probabilities of the excited level with growing density (see Fig. 3). Dissolving of the excited state

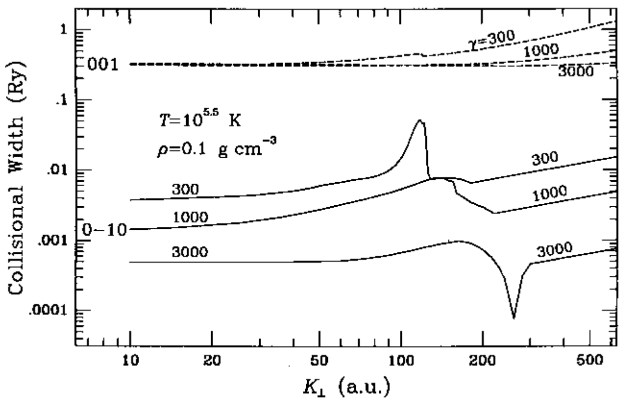

FIG. 4.—Collisional widths $\Gamma_{\kappa\kappa'}(K_\perp)$ of transitions from the ground state to the states $\kappa' = |0\ -1\ 0\rangle$ (*solid lines*) and $|0\,0\,1\rangle$ (*dashed lines*) for $\gamma = 300$, 1000, and 3000.

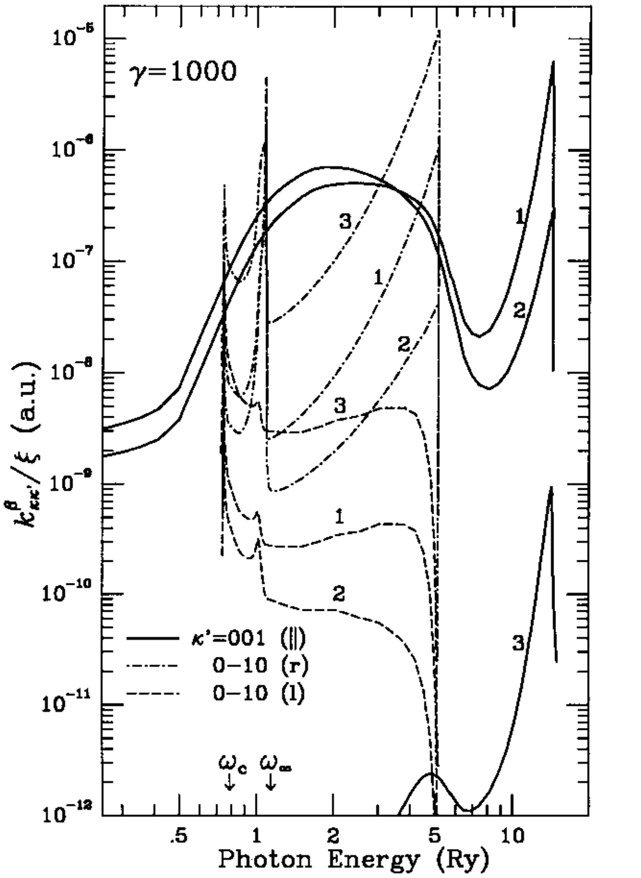

FIG. 5.—Spectral profiles of the absorption coefficient $k^{\beta}_{\kappa\kappa'}(\omega)$ (in atomic units $a_0^{-1} = m_e e^2/\hbar^2$, per unit neutral fraction ξ) for main transitions from the ground state $\kappa = |0 0 0\rangle$ at $B = 2.35 \times 10^{12}$ G. The numbers near the curves correspond to three temperature-density sets: (1) $T = 10^{5.5}$ K, $\rho = 0.01$ g cm^{-3}; (2) $T = 10^6$ K, $\rho = 0.01$ g cm^{-3}; and (3) $T = 10^{5.5}$ K, $\rho = 0.1$ g cm^{-3}.

$|0\ 0\ 1\rangle$ by the microfields of the surrounding ions reduces drastically the height of the peak for the longitudinal polarization (solid curve 3). For the right polarization, this effect is less important because the state $|0\ -1\ 0\rangle$ is tightly bound, so that absorption grows with density in the considered density range.

The spectral features for the circular polarizations near $\hbar\omega_c = 0.74$ Ry and $\hbar\omega_\infty = 1.1$ Ry in Figure 5 are associated with the singularities (26) and (27). The latter one is due to strongly decentered atoms; it is suppressed by the factor $w_{0-10}(K^i_\omega)$ at large K^i_ω (at strong decentering). For $\beta = -1$, this singularity is additionally suppressed by the fast decrease of the oscillator strength $f^{-1}_{\kappa\kappa'}$ at $K_\perp \gg K_c$ (Fig. 2). The decrease of this oscillator strength at $K_\perp \rightarrow 0$, in accordance with the selection rules for axisymmetric magnetized atoms, explains the absence of the peak at the high-energy edge, $\hbar\omega_0 = 5.1$ Ry. The strongly decentered atoms also cause the broad maxima in the absorption profiles for the longitudinally polarized photons at low frequencies (around $\hbar\omega \sim 2$–3 Ry for $\rho = 0.01$ g cm^{-3}). The absorption coefficient grows with decreasing ω because of the increase of $K^i_\omega\,|dK^i_\omega/d\omega|$ at $\omega \rightarrow 0$ (see eq. [28]); the growth evolves into exponential fall at $\hbar\omega \sim 2$ Ry$[(256\pi/3)(N_p a_0)^3]^{1/2}$ (~ 1 Ry for $\rho = 0.01$ g cm^{-3}) because of the decrease of $w_{001}(K^i_\omega)$. The profiles fall down more slowly at very low frequencies, where the tails of the collisional (Lorentz) broadening of the sharp peaks at $\omega = \omega_0$ prevail over the contribution from the decentered atoms. The features at ω_c for

$\beta = \pm 1$ and the high-energy edges of the profiles for $\beta = +1$ and $\beta = 0$ are smoothed by the collisional broadening. The collisional widths (Fig. 4) grow with temperature and density, remaining, however, much smaller than the magnetic widths.

The total coefficient of absorption by atoms on the level κ is given by the sum $k_\kappa^\beta = \sum_{\kappa'} k_{\kappa\kappa'}^\beta$. Since the absorption spectra of the individual transitions are very broad, they essentially overlap in the summed spectrum, contrary to the case of usual, nonmagnetized gas. Figure 6 shows the absorption of the longitudinally polarized photons by atoms on the ground level for two magnetic field strengths, $B = 7 \times 10^{11}$ and 7×10^{12} G, and two temperatures, $T = 10^{5.5}$ and 10^6 K at the density $\rho \approx MN = 0.01$ g cm^{-3}. Transitions to the hydrogen-like states with $\nu > 1$ do not contribute at this density because these states are almost completely destroyed by the plasma microfields. The total absorption at the highest field, $\gamma = 3000$, is almost entirely determined by the main transition $|0\ 0\ 0\rangle \rightarrow |0\ 0\ 1\rangle$. At $\gamma = 300$, the transitions to the states $|0\ -1\ 1\rangle$ and $|0\ -2\ 1\rangle$ do contribute to the total absorption profile. The complicated shape for the latter transition reflects complex $K_\perp$-dependence of the oscillator strength and of the atomic size in this state because of the anticrossings mentioned in § 3. With increasing B and T, population of the decentered atoms grows at the expense of diminishing population of the centered atoms so that the peaks at $\omega \approx \omega_0$ become weaker relative to the low-frequency peaks caused by the decentered atoms. The wide minimum at intermediate frequencies is much deeper at the lower B in both partial and total absorption profiles because of stronger depression of the oscillator strengths at $K_\perp \sim K_c$.

Figures 7 and 8 present absorption of circularly polarized radiation for different magnetic fields, temperatures, and densities. The dependences on the parameters T and ρ are qualitatively the same as in Figure 5. However, the apparent shapes of the spectra are quite different at different field strengths because the $K_\perp$-dependence of the oscillator strengths and binding energies becomes smoother at higher B and their dependence on the quantum number m' becomes more pronounced. In particular, since the tightly bound excited levels are more distant from each other than the hydrogen-like levels, the contributions from the individual transitions are more distinctive than in Figure 6, especially at the highest field $\gamma = 3000$. In spite of their generally lower rates, the transitions to $|0\ m'\ 0\rangle$, with $m' < 0$, are seen clearly in the summarized spectral profiles as additional relatively broad peaks at higher energies. They also give rise to narrow spikes at harmonics of the proton cyclotron frequency; the spikes are associated with the singularities at ω_∞ discussed above.

5. SUMMARY AND CONCLUSIONS

The coupling of the center-of-mass and internal atomic motions in strong magnetic fields causes a great redward broadening of spectral lines absorbed or emitted by the hydrogen gas. For realistic temperatures, this *magnetic broadening* transforms the discrete absorption or emission spectrum into a

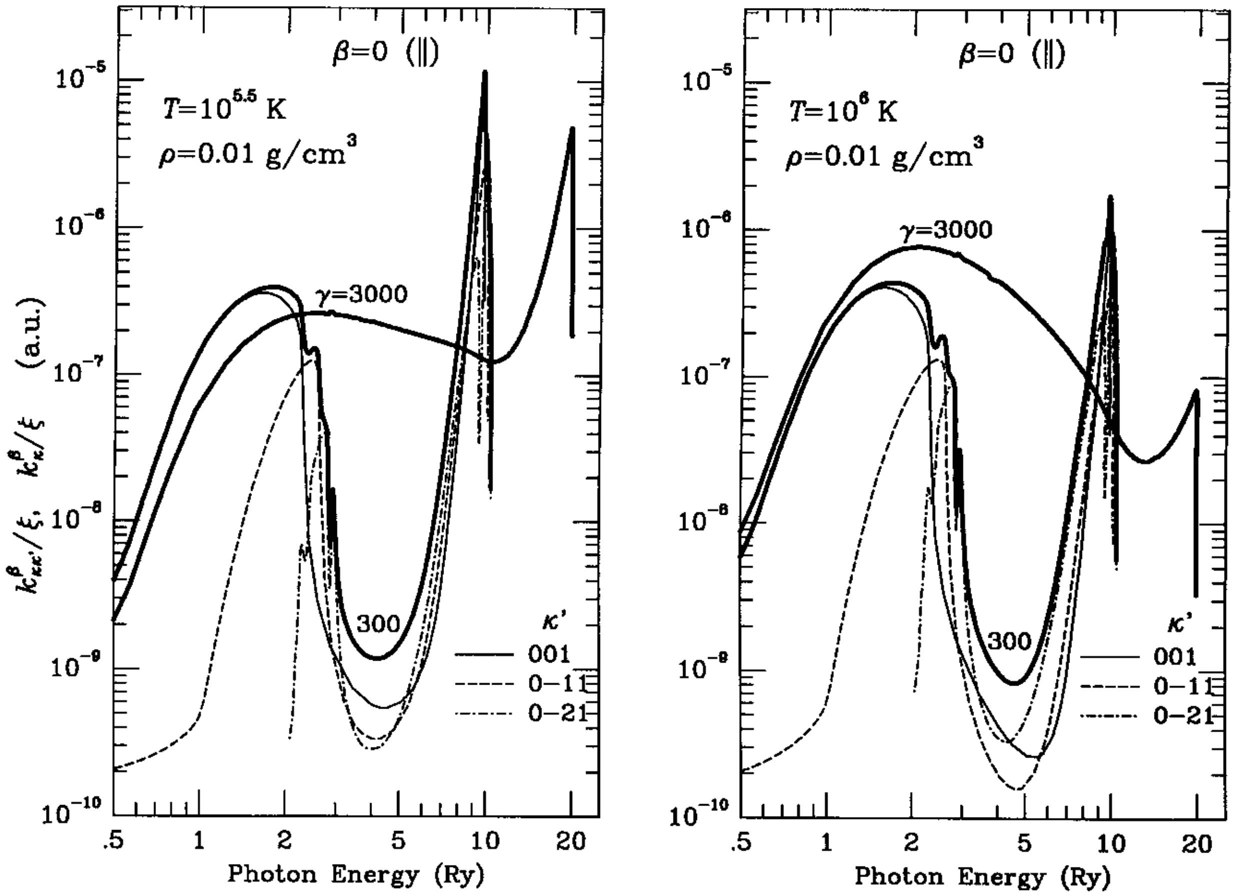

FIG. 6.—Spectral profiles of partial (*thin lines*) and total (*thick lines*) absorption coefficients for longitudinally polarized photons at $\rho = 0.01$ g cm^{-3} for different values of magnetic field and temperature.

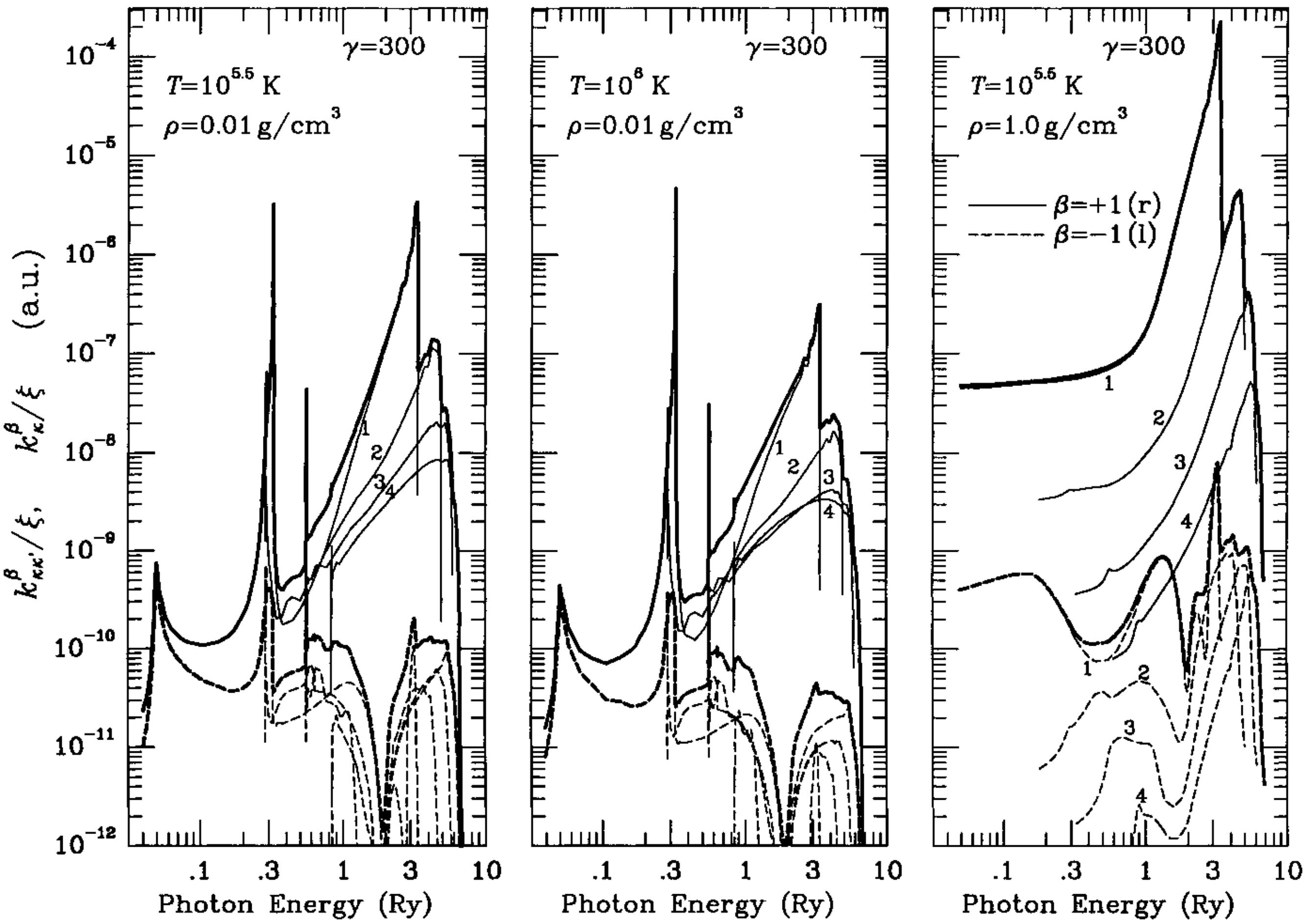

FIG. 7.—Absorption profiles for circularly polarized photons at $B = 7 \times 10^{11}$ G for different values of temperature and density. The lines are labeled by the quantum numbers $(-m')$ of the final states $\kappa' = |0\, m'\, 0\rangle$; the thick lines correspond to the total absorption.

continuum. For densities and temperatures that are not too high, the spectra can be considered as consisting of two components provided by two populations of the hydrogen atoms, as we discuss in detail below.

The *high-energy component* is generated by the bound-bound transitions in *centered atoms* which have small transverse generalized momenta, $K_\perp \ll K_c$, where K_c is a critical value associated with restructuring of the atoms at varying $K_\perp$. The spectral profiles of the high-energy component can be described approximately in the frame of the perturbation theory (Pavlov & Mészáros 1993). For each separate transition, the spectrum has a high-energy edge, slightly smoothed by the collisional and Doppler broadening, and a wide tail decreasing redward. In accordance with the selection rules for the centered atoms, the main transitions from the ground level $|0\ 0\ 0\rangle$ are those to the hydrogen-like level $|0\ 0\ 1\rangle$ for the longitudinal polarization and to the tightly bound level $|0\ -1\ 0\rangle$ for the right circular polarization; for typical neutron star magnetic fields, the absorptions are peaked at soft X-ray (0.1–0.3 keV) and EUV (40–100 eV) ranges, respectively. Absorption of photons with the left circular polarization by the centered atoms in the ground state is forbidden by the selection rules unless the photon energy is comparable to, or exceeds, the electron cyclotron energy. Interaction of the atoms with surrounding particles (nonideality effects) in the dense plasmas of the neutron star atmospheres can suppress the high-energy component; this effect is especially strong for the longitudinal polarization.

The *low-energy component* is provided by transitions in *decentered atoms* ($K_\perp \gtrsim K_c$). For the longitudinal polarization, it appears as a broad peak centered at an energy determined by the nonideality effects. For realistic densities and temperatures, this peak lies in the UV/EUV range ($\sim$5–50 eV). For the right circular polarization, the low-energy component lies mainly redward of its main peak near the proton cyclotron energy, $\hbar\omega_{Bp} = 6.3(B/10^{12}\text{ G})$ eV; the peak is caused by transitions in strongly decentered atoms ($K_\perp \gg K_c$). It is limited from the side of low energies by the minimum space $\hbar\omega_c$ between the upper and lower atomic levels in the course of their anticrossing at $K_\perp \simeq K_c$. The value of $\hbar\omega_c$ depends strongly on the magnetic field strength, varying from IR/optical energies at lower fields to EUV at higher fields. For the left circular polarization, the bound-bound absorption from the ground level to the levels $|0\ m'\ v'\rangle$ is forbidden for both centered and strongly decentered atoms, so that the absorption concentrates in a narrow energy range near ω_c.

Thus, the bound-bound transitions contribute to absorption and emission of radiation in a wide energy range, from optical to soft X-ray energies. Because of the great magnetic broadening, one cannot expect narrow spectral lines in the thermal-like neutron star radiation even if it is emitted from a region of a nearly uniform magnetic field. Since the cumulative oscillator

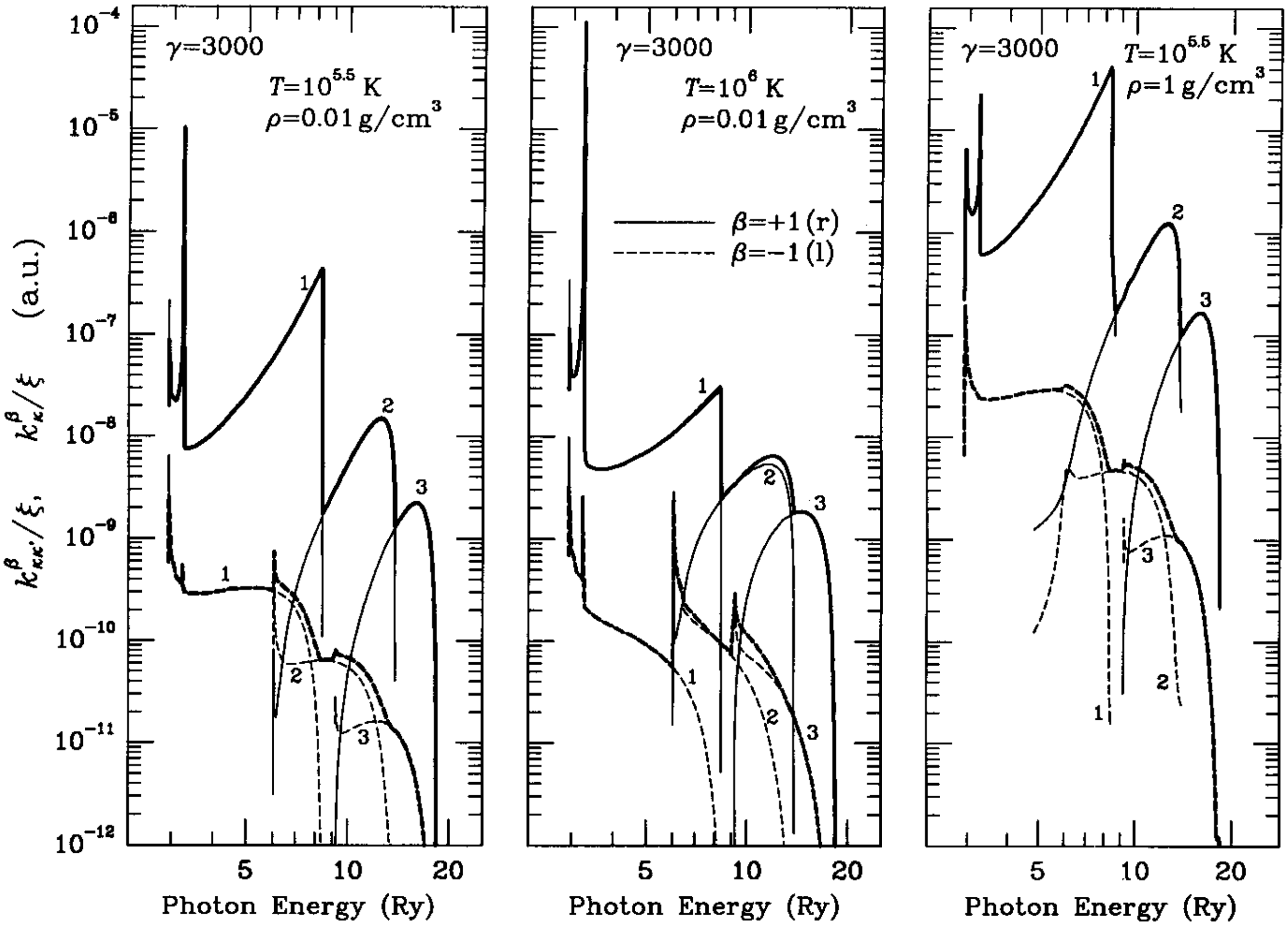

FIG. 8.—Same as in Fig. 7 for $B = 7 \times 10^{12}$ G

strength of the bound-bound transitions is comparable to the integral oscillator strength for the photoionization (Miller & Neuhauser 1991), the bound-bound transitions may be as important in the continuum absorption as the bound-free ones. The combined effect of the bound-bound and bound-free transitions should lead to rather broad absorption features (depressions) in the soft X-ray/UV spectra of neutron star atmospheres. The equivalent widths of these features are determined by relative contributions of the atomic absorption and absorption by magnetized "free" electrons and protons. These contributions depend significantly on the ionization equilibrium in the dense strongly magnetized plasmas, a problem that requires accurate investigation with allowance for the nonideality effects and decentering of the moving atoms (Pavlov et al. 1995). Comparison of the obtained bound-bound absorption coefficients with the electron free-free absorption coefficients (e.g., Kaminker, Pavlov, & Shibanov 1983),

$$k_{\rm ff}^{0} \simeq 1.1 \times 10^{-9} a_0^{-1} \left(\frac{\rho}{10^{-2}\ {\rm g\ cm^{-3}}}\right)^{2} \left(\frac{T}{10^{6}\ {\rm K}}\right)^{-1/2} \times \left(\frac{\hbar\omega}{10\ {\rm Ry}}\right)^{-3} (1 - e^{-\hbar\omega/kT}) \Lambda_{\parallel}\,, \quad (29)$$

$$k_{\rm ff}^{\pm 1} \simeq (\omega/\omega_B)^2 (\Lambda_{\perp}/\Lambda_{\parallel}) k_{\rm ff}^{0}\,, \quad (30)$$

where $\Lambda_{\parallel,\perp}$ are the Coulomb logarithms, shows that the bound-bound absorption is of major importance even if the neutral fraction is as small as $\sim 10^{-5}$ to 10^{-3}. The atomic absorption is especially important for the transverse polarizations, $\beta = \pm 1$, since the corresponding bound-bound coefficients are much less suppressed by the strong magnetic fields than the free-free ones. Since the frequency dependence of the absorption coefficients is substantially different for photons of different polarizations, and the contributions of the polarizations to the radiation emitted from a neutron star atmosphere depend on the orientation of the magnetic field, one can expect a noticeable dependence of the emitted spectra on the orientation of the neutral star magnetic axis with respect to the line of sight. In other words, the light curves should look quite different in different parts of the observed spectra. This and other effects of the bound-bound transitions in the strongly magnetized plasmas should be taken into account in modeling and interpretation of the thermal-like soft X-ray/UV/optical radiation from cooling neutron stars.

One of the authors (A. Y. P.) expresses gratitude to all the Nordita staff and especially to C. J. Pethick for the hospitality and excellent working conditions during the visits to Nordita in 1993 and 1994. A. Y. P.'s visit to Nordita in 1994 was supported in part by the Nordic Council of Ministers' Scholarship Programme for the Baltic Region and North-West Russia. This work was partially supported by Russian Foundation for Fundamental Research (grant 93-02-2916), by ISF grant R6A000, and by NASA Astrophysics Theory Program (grant NAG5-2807).

APPENDIX

IMPACT BROADENING

The collisional width due to impact of the atom with plasma electrons can be estimated as (see, e.g., Sobelman, Vainshtein, & Yukov 1981)

$$\Gamma_{\kappa\kappa'}(K_\perp) = 2N_e\langle\sigma v\rangle . \tag{A1}$$

Here v is the electron velocity, $N_e(=N_p)$ is the electron number density, and σ is the width effective cross section. In the isotropic case, the cross section can be estimated as $\sigma \simeq \pi\rho_{\mathrm{W}}^2$; the Weisskopf radius ρ_{W} is the impact parameter defined by the condition $|\eta| = 1$, where

$$\eta = \int_{-\infty}^{\infty} \Delta\omega_{\kappa'\kappa}(t)dt , \tag{A2}$$

is the phase shift, and $\Delta\omega_{\kappa'\kappa}(t)$ is the instantaneous shift of the transition frequency due to interaction with the perturbing electron,

$$\hbar\Delta\omega_{\kappa'\kappa} = \Delta\chi_\kappa - \Delta\chi_{\kappa'} . \tag{A3}$$

In the case of a strong magnetic field, $\hbar\omega_{\mathrm{B}} \gg k_{\mathrm{B}} T$, the perturbing electrons move along the magnetic field lines (along the z-axis). Moreover, the moving atom is stretched along the direction $\boldsymbol{e}_x$ perpendicular to the transverse momentum $\boldsymbol{K}_\perp = K_\perp \boldsymbol{e}_y$. This means that the value of ρ_{W}, for which $|\eta| = 1$, depends on the azimuthal angle φ of the (rectilinear) electron trajectory with respect to the x-axis, and the cross section can be generalized as

$$\sigma = \tfrac{1}{2}\int_0^{2\pi} d\varphi\, \rho_{\mathrm{W}}^2(\varphi) . \tag{A4}$$

To find $\rho_{\mathrm{W}}(\varphi)$, we consider the energy shift $\Delta\chi_\kappa$ due to the linear and quadratic Stark effect in the electric field $\boldsymbol{F}$ of the perturbing electron,

$$\Delta\chi_\kappa = -eF_\perp \bar{x}_\kappa \cos\varphi + e^2F_\perp^2 \sum_{\kappa''\neq\kappa} \frac{|x_{\kappa''\kappa}\cos\varphi + y_{\kappa''\kappa}\sin\varphi|^2}{\hbar\omega_{\kappa''\kappa}} + e^2F_z^2 \sum_{\kappa''\neq\kappa} \frac{|z_{\kappa''\kappa}|^2}{\hbar\omega_{\kappa''\kappa}} , \tag{A5}$$

where $\bar{x}_\kappa = x_{\kappa\kappa}$ is the mean decentering, and all the matrix elements $x_{\kappa''\kappa}$, etc., are taken between the states $\langle\kappa'', K_\perp|$ and $|\kappa, K_\perp\rangle$. The transverse and longitudinal components of the field are

$$F_\perp = \frac{-e\rho_{\mathrm{W}}}{(\rho_{\mathrm{W}}^2 + v^2t^2)^{3/2}} , \qquad F_z = \frac{-evt}{(\rho_{\mathrm{W}}^2 + v^2t^2)^{3/2}} . \tag{A6}$$

The first term in equation (A5) allows for the linear Stark effect. The corresponding phase shift equals

$$\eta_1 = 2\frac{e^2}{\hbar v}\frac{\bar{x}_{\kappa'} - \bar{x}_\kappa}{\rho_{\mathrm{W}}}\cos\varphi . \tag{A7}$$

The remaining terms in equations (A5) are due to the quadratic Stark effect. It is convenient to express the corresponding phase shift η_2 in terms of the oscillator strengths (9), making the following transformation:

$$|x_{\kappa''\kappa}\cos\varphi + y_{\kappa''\kappa}\sin\varphi|^2 = \tfrac{1}{2}\{|(r_+)_{\kappa''\kappa}|^2 + |(r_-)_{\kappa''\kappa}|^2 + \mathrm{Re}\,[(r_+)_{\kappa''\kappa}(r_+)_{\kappa\kappa''}e^{-2i\varphi}]\} \tag{A8}$$

$$\simeq a_0^2 \frac{\mathrm{Ry}}{2\hbar\omega_{\kappa''\kappa}}(f_{\kappa''\kappa}^{+1} - f_{\kappa\kappa''}^{+1}) . \tag{A9}$$

Here we used the fact that third term in equation (A8) is numerically much smaller than the sum of the first two (it equals exactly zero if m is the exact quantum number) and took into account that $f_{\kappa''\kappa}^{-1} = -f_{\kappa\kappa''}^{+1}$. Using equation (A9), we obtain

$$\eta_2 = \frac{e^2}{\hbar v}\frac{r_{\kappa'}^3 - r_\kappa^3}{\rho_{\mathrm{W}}^3} , \tag{A10}$$

where

$$r_\kappa^3 = \frac{3\pi}{8}a_0^3 \sum_{\kappa''\neq\kappa}\left(\frac{\mathrm{Ry}}{\hbar\omega_{\kappa''\kappa}}\right)^2\left(f_{\kappa''\kappa}^{+1} - f_{\kappa\kappa''}^{+1} + \frac{2}{3}f_{\kappa''\kappa}^{0}\right) . \tag{A11}$$

The equation $|\eta_1 + \eta_2| = 1$ is a cubic equation for $\rho_{\mathrm{W}}(\varphi)$. It can be solved to obtain the cross section according to equation (A4). For a rough estimate, we approximate the cross section as $\sigma \approx \sigma_1 + \sigma_2$, where

$$\sigma_1 = 2\pi\left(\frac{e^2}{\hbar v}\right)^2 |\bar{x}_{\kappa'} - \bar{x}_\kappa|^2 \tag{A12}$$

and

$$\sigma_2 = \pi\left(\frac{e^2}{\hbar v}\right)^{2/3} |r_{\kappa'}^3 - r_\kappa^3|^{2/3} \tag{A13}$$

are provided by the linear and quadratic Stark terms separately [i.e., the corresponding $\rho_{W1}(\varphi)$ and $\rho_{W2}(\varphi)$ are obtained from the equations $|\eta_1| = 1$ and $|\eta_2| = 1$, respectively]. Substituting the cross section into equation (A1) gives

$$\Gamma_{\kappa\kappa'}(K_\perp) \approx 4\pi N_e\left(\frac{e^2}{\hbar}\right)^2 |\bar{x}_{\kappa'} - \bar{x}_\kappa|^2\langle v^{-1}\rangle + 2\pi N_e\left(\frac{e^2}{\hbar}\right)^{2/3} |r_{\kappa'}^3 - r_\kappa^3|^{2/3}\langle v^{1/3}\rangle \,. \tag{A14}$$

Averaging of v^{-1} with the *one-dimensional* Maxwell distribution leads to an integral diverging logarithmically at $v = 0$. In fact, however, the impact approximation is inapplicable for slow electrons. It is well known (see, e.g., Sobelman et al. 1981) that the approximation can be used for frequencies that are closer to the line center than the inverse duration of collision, $\Delta\omega \ll v/\rho$, where ρ is a typical impact parameter. The cutoff velocity $v_{\rm min}$ can be found from the condition that a substantial part of the line contour, $\Delta\omega \sim 2\pi\rho_W^2 N_e v$, can be described by the impact approximation. This condition is equivalent to $N_e\rho_W^3 \ll 1$, i.e., the Weisskopf radius is much smaller than the mean distance between the perturbers (the condition of binary collisions). Adopting $\rho_W \sim \rho_{W1} \sim (e^2/\hbar v)|\bar{x}_{\kappa'} - \bar{x}_\kappa|$, we obtain

$$v_{\rm min} \sim (e^2/\hbar)N_e^{1/3}|\bar{x}_{\kappa'} - \bar{x}_\kappa| \,. \tag{A15}$$

Thus, the mean values in equation (A14) are

$$\langle v^{-1}\rangle = \left(\frac{m_e}{2\pi k_B T}\right)^{1/2} E_1\left(\frac{m_e v_{\rm min}^2}{2k_B T}\right) \quad \text{and} \quad \langle v^{1/3}\rangle = \frac{1}{\sqrt{\pi}}\left(\frac{2k_B T}{m_e}\right)^{1/6}\Gamma\left(\frac{2}{3}\right), \tag{A16}$$

where $E_1(x)$ ($\simeq -\ln x - 0.58$ at $x \ll 1$) is the integral exponent, and $\Gamma(\frac{2}{3}) \simeq 1.35$ is the gamma function. With these values, the impact width equals

$$\Gamma_{\kappa\kappa'}(K_\perp) \simeq N_e\frac{e^2}{\hbar}\left[7.1|\bar{x}_{\kappa'} - \bar{x}_\kappa|^2\left(\frac{k_B T}{\rm Ry}\right)^{-1/2} E_1\left(\frac{\rm Ry}{k_B T}|\bar{x}_{\kappa'} - \bar{x}_\kappa|^2 N_e^{2/3}\right) + 4.8|r_{\kappa'}^3 - r_\kappa^3|^{2/3}\left(\frac{k_B T}{\rm Ry}\right)^{1/6}\right]. \tag{A17}$$

This equation is used to calculate the line contours.

It should be noted that, rigorously speaking, the continuum part of the perturbational basis cannot be fully ignored in calculation of r_κ and $r_{\kappa'}$ with equation (A11). The main contribution to r_{0m0} comes from $f^0_{0m1,0m0}$, but the states $|\kappa''\rangle = |0\ m\ 1\rangle$ with $m \neq 0$ are involved into the continuum at sufficiently large $K_\perp$ and/or γ. Accurate treatment of such metastable states is rather complicated; however, they can be easily treated using the adiabatic approximation. A comparison of such a simplified approach with a more accurate (although approximate) one (Potekhin 1994) for a few metastable states shows that the adiabatic approximation provides an accuracy of $\Gamma_{\kappa\kappa'}(K_\perp)$ not worse than tens of percent, which is quite satisfactory for our goals. Therefore, we used the adiabatic approximation in equation (A11) whenever more accurate results were inaccessible.

At $K_\perp \ll \gamma\hbar/a_0$, when the atoms are well centered, the values of $\bar{x}_\kappa$ and $\bar{x}_{\kappa'}$ are negligibly small so that the broadening is entirely determined by the quadratic Stark effect and the main contribution is provided by the Stark shift of the excited level,

$$\Gamma_{\kappa\kappa'}(K_\perp) \approx 4.8(N_e e^2/\hbar)(k_B T/{\rm Ry})^{1/6} r_{\kappa'}^2 \,. \tag{A18}$$

For the transitions from the ground level, the final states are tightly bound ($m' = -1$, $v' = 0$) and hydrogen-like ($m' = 0$, $v' = 1, 3, \ldots$) for the transverse (right) and longitudinal polarization, respectively. The hydrogen-like levels can be easily mixed with the adjacent levels $m'' = 0$, $v'' = v' + 1$ by the longitudinal electric field. The tightly bound levels, on the contrary, are much more isolated, and the dipole matrix elements mixing these levels with neighboring ones are much smaller. As a result, the width is much smaller for the transverse polarization than for the longitudinal polarization (see Fig. 4).

When the atom is strongly decentered ($K_\perp > \gamma\hbar/a_0$), the computation of the width (eq. [A17]) is complicated because the parameters r_κ and $r_{\kappa'}$, as well as $\bar{x}_\kappa$ and $\bar{x}_{\kappa'}$, become similar and nearly compensate each other. The compensation results in a rapid decrease of σ_1 with increasing $K_\perp$. On the contrary, $|r_{\kappa'}^3 - r_\kappa^3|$ keeps growing with $K_\perp$. In order to estimate $r_{\kappa'}^3 - r_\kappa^3$ analytically, let us notice that for the decentered states ($K_\perp > K_c$) the main contribution to equation (A11) comes from the quadratic Stark terms with $\kappa'' = (0, m, v \pm 1)$:

$$r_{0mv}^3 \approx \frac{\pi e^2}{8}\left(\frac{|z_{0mv+1,0mv}|^2}{\chi_{0mv} - \chi_{0mv+1}} - \frac{|z_{0mv,0mv-1}|^2}{\chi_{0mv-1} - \chi_{0mv}}\right). \tag{A19}$$

If we make use of the shifted adiabatic approximation (well justified at $K_\perp \gg K_c$, see Potekhin 1994) and expand the effective potential $V_{0m}(z)$ over inverse powers of r_c [that leads to asymptotic series applicable at $K_\perp \gg \gamma\hbar(v + \frac{1}{2})^2/a_0$], we obtain the oscillator-like potential of Burkova et al. (1976) with m-dependent and anharmonic corrections:

$$V_{0m}(z) = -\frac{e^2}{r_c}\left\{1 + \frac{1-m}{2}\frac{a_m^2}{r_c^2} - \left[1 + \frac{9}{2}(1-m)\frac{a_m^2}{r_c^2}\right]\frac{z^2}{2r_c^2} + \frac{3z^4}{8r_c^4}\right\}, \tag{A20}$$

where $a_m = a_0/\gamma^{1/2}$ is the magnetic length. Treating the corrections as small perturbation yields

$$E^{\parallel}_{0m\nu} = -\frac{e^2}{r_c}\left\{1 + \frac{1-m}{2}\frac{a_m^2}{r_c^2} - \sqrt{\frac{a_0}{r_c}}\left[1 + \frac{9}{4}(1-m)\frac{a_m^2}{r_c^2}\right]\left(\nu + \frac{1}{2}\right) + \frac{9}{16}\frac{a_0}{r_c}\left(\nu^2 + \nu + \frac{1}{2}\right)\right\}, \tag{A21}$$

and

$$z_{0m\nu,0m\nu-1} = (a_0 r_c^3)^{1/4}\left[1 + \frac{9\nu}{16}\sqrt{\frac{a_0}{r_c}} - \frac{9}{8}(1-m)\frac{a_m^2}{r_c^2}\right]\sqrt{\frac{\nu}{2}}. \tag{A22}$$

In equations (A21) and (A22) only those small terms are retained which give the leading m- and ν-dependent contributions to equation (A19):

$$r^3_{0m\nu} \approx \frac{\pi r_c^3}{16}\left\{1 + \frac{9}{2}\left[\left(\nu + \frac{1}{2}\right)\sqrt{\frac{a_0}{r_c}} - (1-m)\frac{a_m^2}{r_c^2}\right]\right\}. \tag{A23}$$

Thus we have, in particular, $r_{00\nu} \approx (\nu^2 a_0 r_c^5)^{1/6}$ and $r_{0m0} \approx (|m| a_m^2 r_c)^{1/3}$.

REFERENCES

Bezchastnov, V. G., & Potekhin, A. Y. 1994, J. Phys. B, 27, 3349
Burkova, L. A. Dzyaloshinskii, I. E., Drukarev, G. F., & Monozon, B. S. 1976, Zh. Eksper. Teoret. Fiz., 71, 526 (Soviet Phys.—JETP, 44, 276)
Canuto, V., & Ventura, J. 1977, Fundam. Cosmic Phys., 2, 203
Forster, H., Strupat, W., Rösner, W., Wunner, G., Ruder, H., & Herold, H. 1984, J. Phys. B, 17, 1301
Gorkov, L. P., & Dzyaloshinskii, I. E. 1967, Zh. Eksper. Teoret. Fiz., 53, 717 (1968 Soviet Phys.—JETP, 26, 449
Hummer, D. G., & Mihalas, D. 1988, ApJ, 331, 794
Kaminker, A. D., Pavlov, G. G., & Shibanov, Yu. A. 1983, Ap&SS, 91, 167
Miller, M. C., & Neuhauser, D. 1991, MNRAS, 253, 107
Ögelman, H. 1995, in The Lives of the Neutron Stars, ed. A. Alpar, Ü. Kiziloğlu, & J. van Paradijs (Dordrecht: Kluwer), 101
Pavlov, G. G., & Mészáros, P. 1993, ApJ, 416, 752
Pavlov, G. G., Shibanov, Yu. A., Zavlin, V. E., & Meyer, R. D. 1995, in The Lives of the Neutron Stars, ed. A. Alpar, Ü. Kiziloğlu, & J. van Paradijs (Dordrecht: Kluwer), 71
Potekhin, A. Y. 1994, J. Phys. B, 27, 1073
Potekhin, A. Y., & Pavlov, G. G. 1993, ApJ, 407, 330
Sobelman, I. I., Vainshtein, L. A., & Yukov, E. A. 1981, Excitation of Atoms and Broadening of Spectral Lines (Berlin: Springer)
Stehlé, C., & Jacquemot, S. 1993, A&A, 271, 348
Ventura, J., Herold, H., & Kopidakis, N. 1995, in The Lives of the Neutron Stars, ed. A. Alpar, Ü. Kiziloğlu, & J. van Paradijs (Dordrecht: Kluwer), 97
Ventura, J., Herold, H., Ruder, H., & Geyer, F. 1992, A&A, 261, 235
Vincke, M., & Baye, D. 1988, J. Phys. B, 21, 2407
Vincke, M., Le Dourneuf, M., & Baye, D. 1992, J. Phys. B, 25, 2787